Electronic Supplementary Material (ESI) for CrystEngComm.

Supporting Information

New isomeric $Ni(NCS)_2$ coordination compounds: crystal structures, magnetic properties and *ex situ* as well as *in situ* investigations on their synthesis and transition behaviour

Carsten Wellm, Tristan Neumann, Magdalena Ceglarska, Gianpiero Gallo,

Michał Rams, Robert E. Dinnebier and Christian Näther

Content

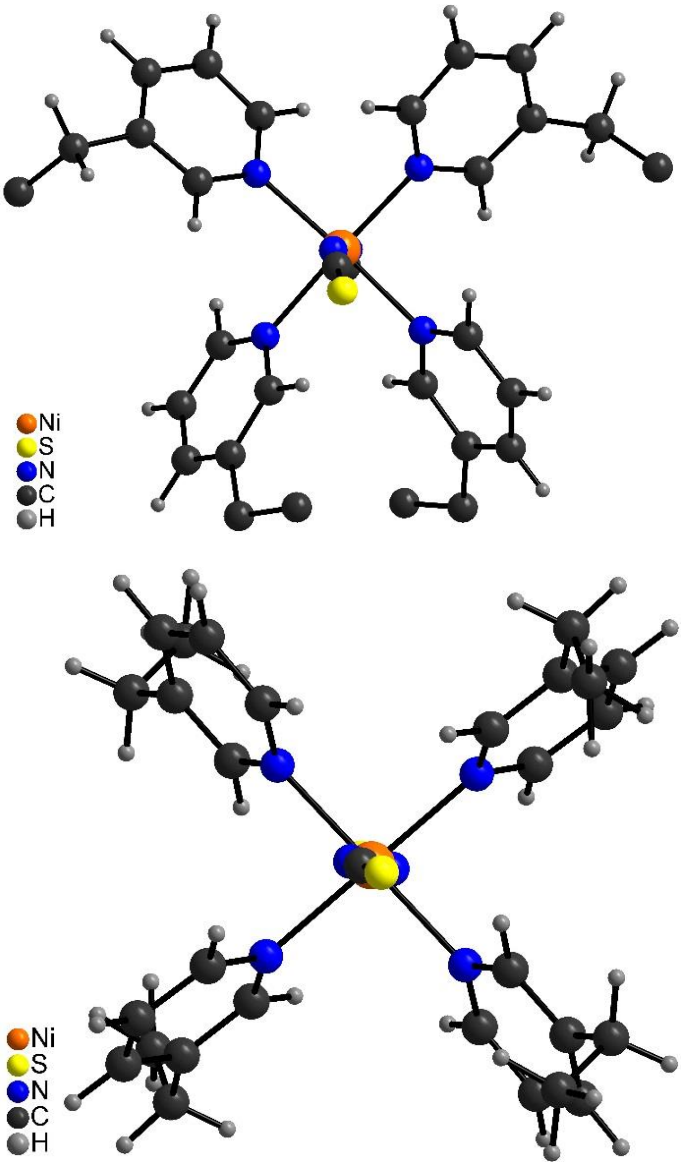

Figure S1. Crystal structures of **1-I** (top) and of **1-II** (bottom) retrieved from literature with view of the Ni coordination. Please note that for **1-I** no coordinates for the methyl H atoms are given.

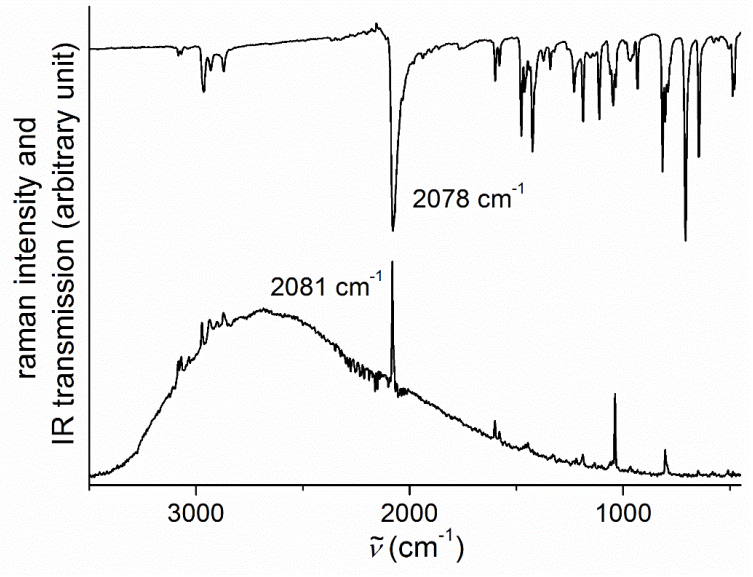

Figure S2. IR and Raman spectra of **1-I**. Given are the values for the CN stretching vibrations.

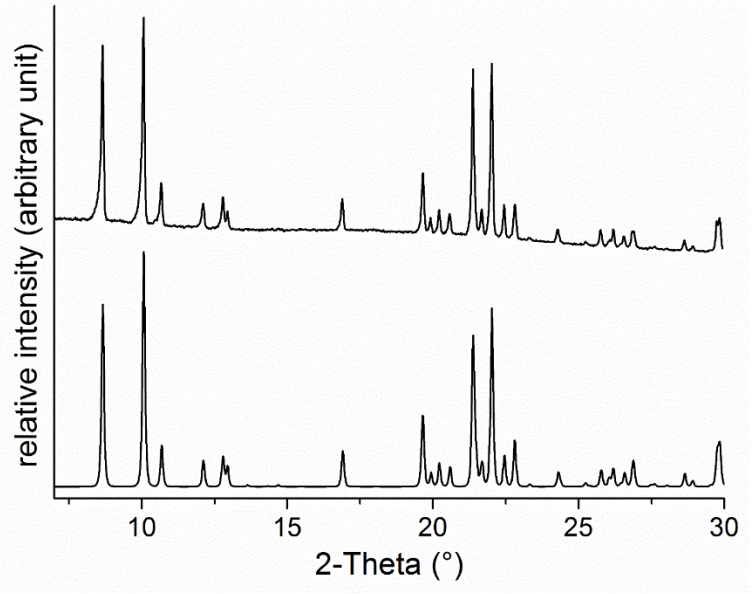

Figure S3. Experimental (top) and calculated (bottom) XRPD pattern of **1-I**.

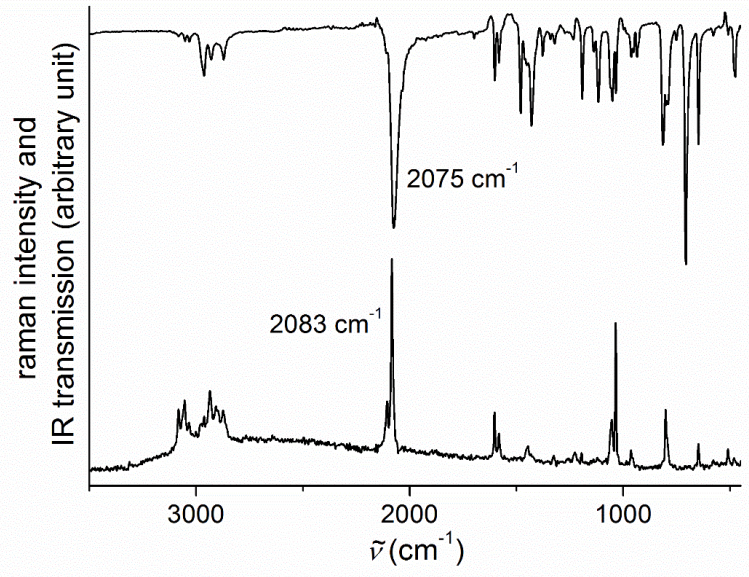

Figure S4. IR and Raman spectra of **1-II**. Given are the values for the CN stretching vibrations.

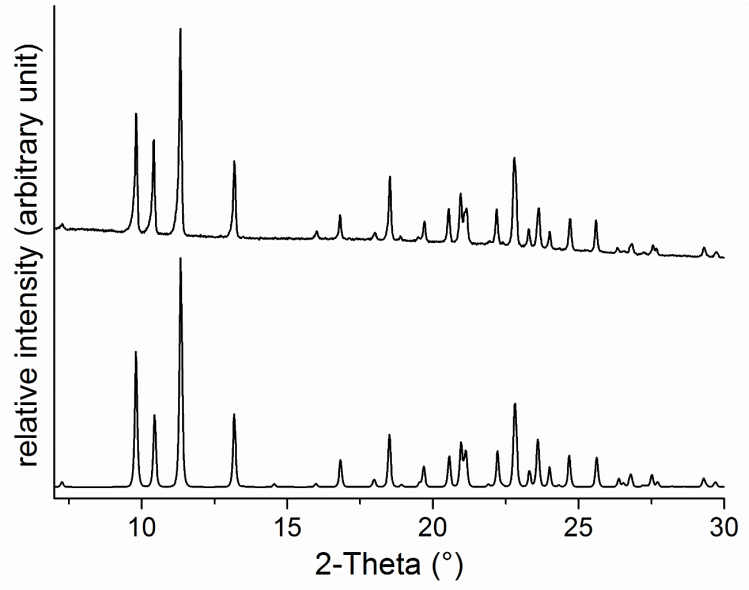

Figure S5. Experimental (top) and calculated (bottom) XRPD pattern of **1-II**.

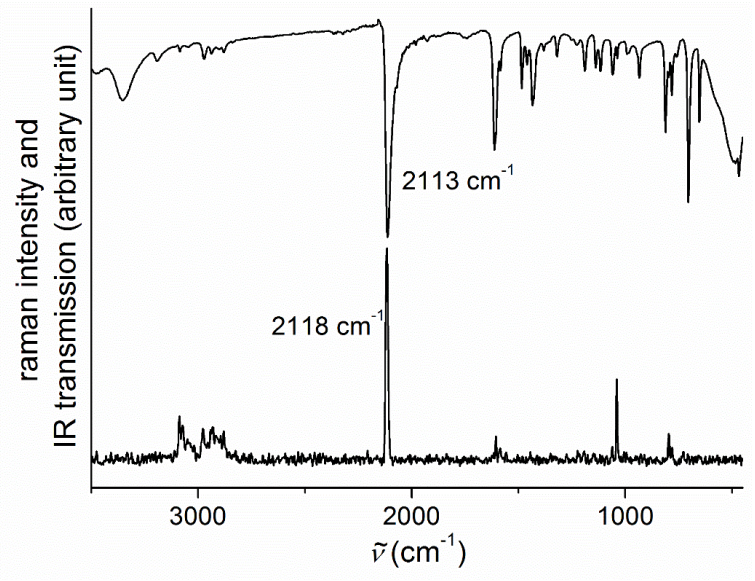

Figure S6. IR and Raman spectra of **2**. Given are the values for the CN stretching vibrations.

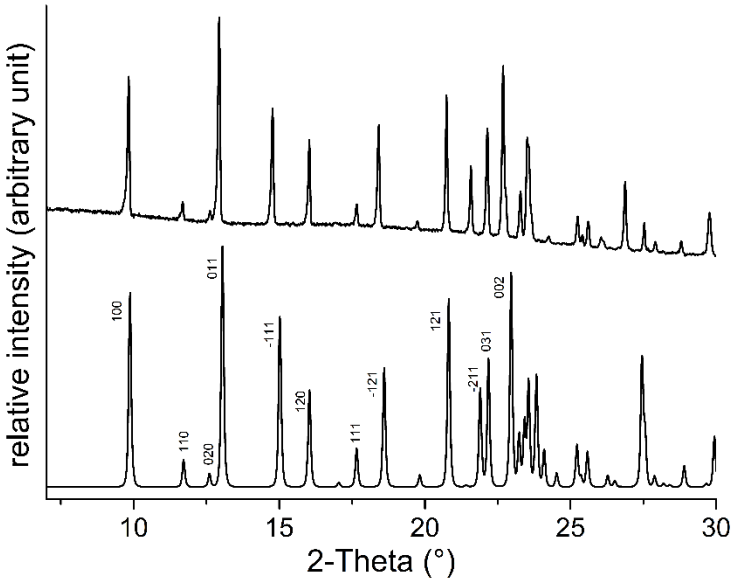

Figure S7. Experimental (top) and calculated (bottom) XRPD pattern of **2**. For the calculated pattern some indices are given.

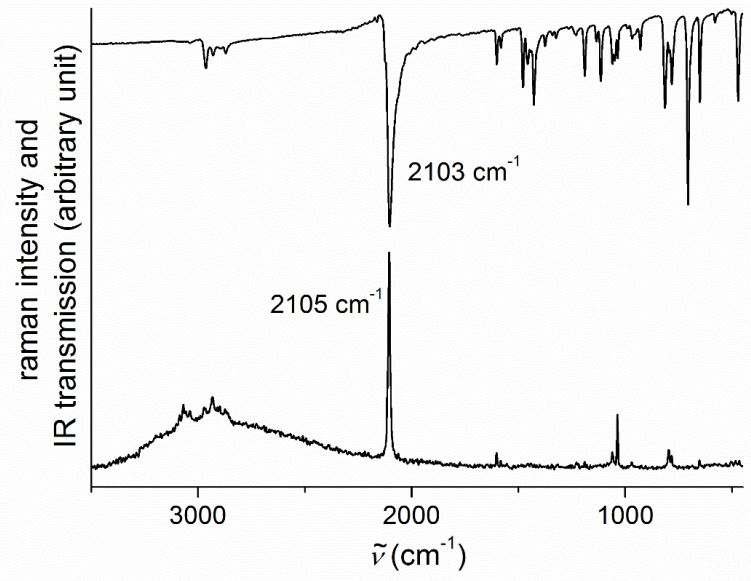

Figure S8. IR and Raman spectra of **3-lc**. Given are the values for the CN stretching vibrations.

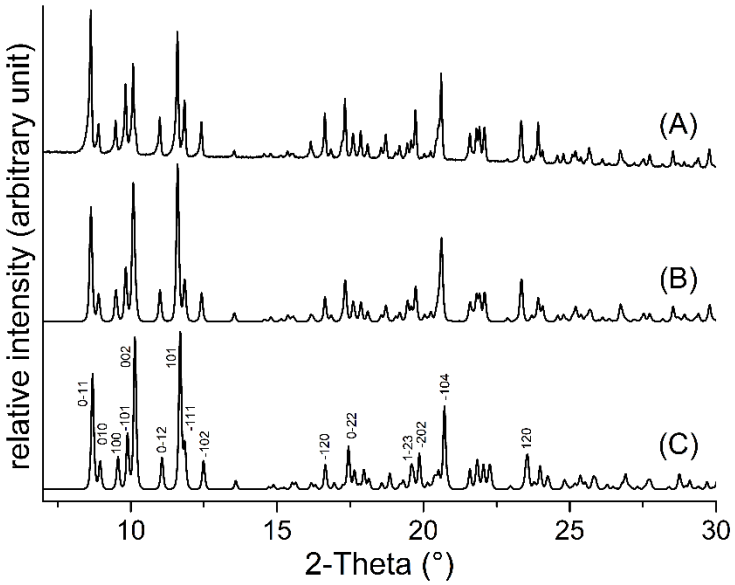

Figure S9. Experimental (A) and calculated XRPD pattern using the lattice parameters obtained from a pawley fit of a powder pattern measured at room temperature (B) and using the lattice parameters from single crystal data measured at 200 K of **3-lc** (C). For the calculated pattern some indices are given.

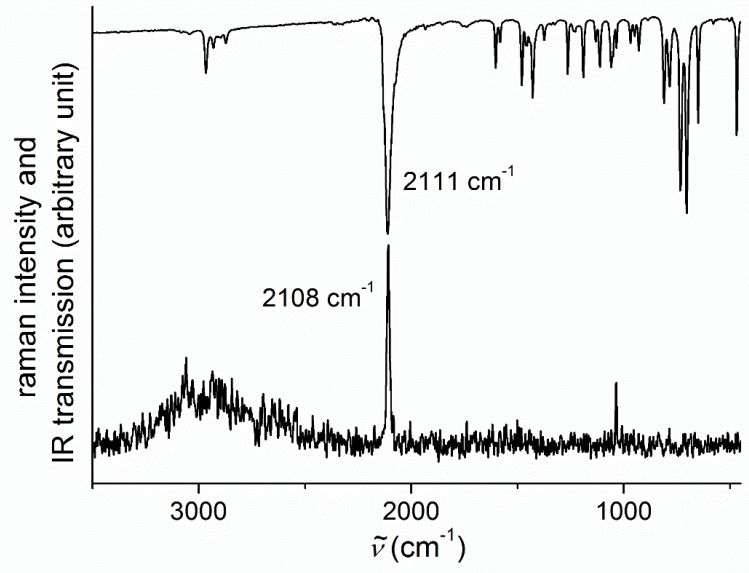

Figure S10. IR and Raman spectra of **3c-CH_2Cl_2**. Given are the values for the CN stretching vibrations.

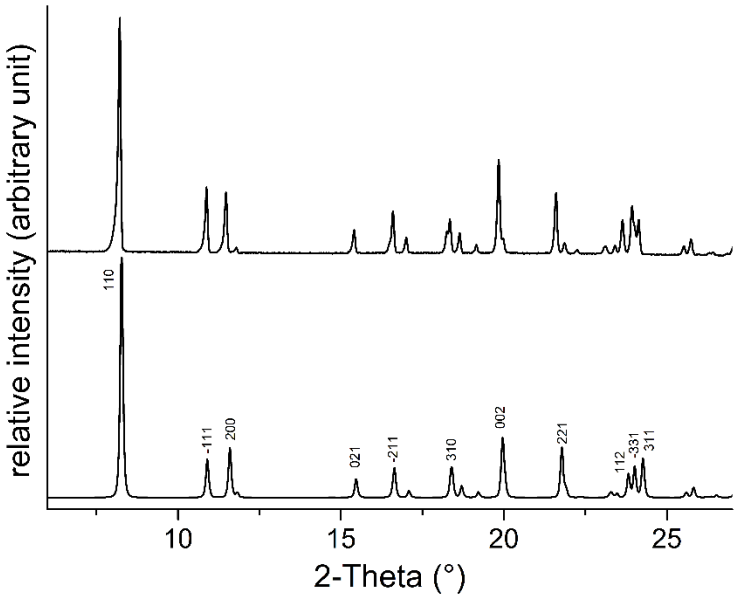

Figure S11. Experimental (top) and calculated (bottom) XRPD pattern of **3c-CH_2Cl_2**. For the calculated pattern some indices are given.

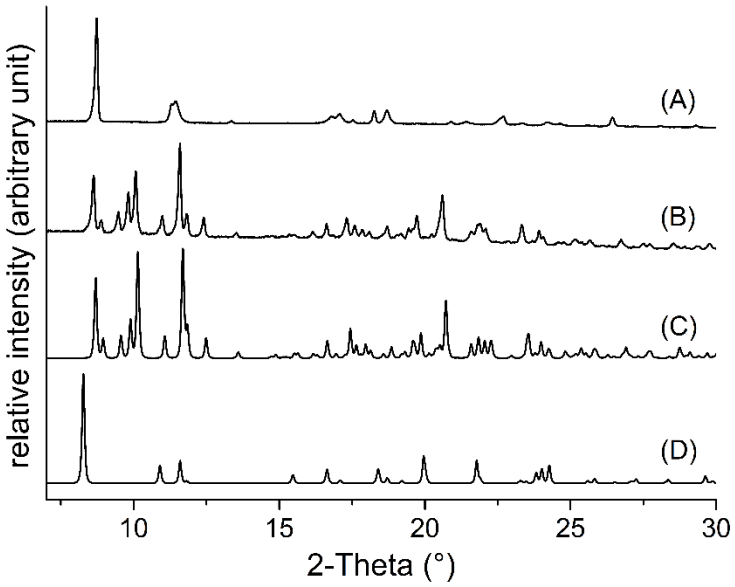

Figure S12. Experimental XRPD pattern of the residue that is obtained if **3c-CH_2Cl_2** kept at ambient condition for one day (A) and after several months (B) together with the calculated patterns of **3-lc** (C) and **3c-CH_2Cl_2** (D).

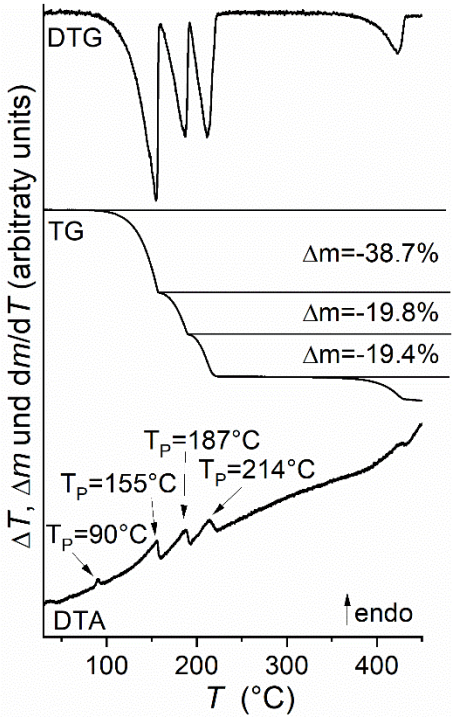

Figure S13. DTG, TG and DTA curve for **1-II** measured with a heating rate of 1°C/min.

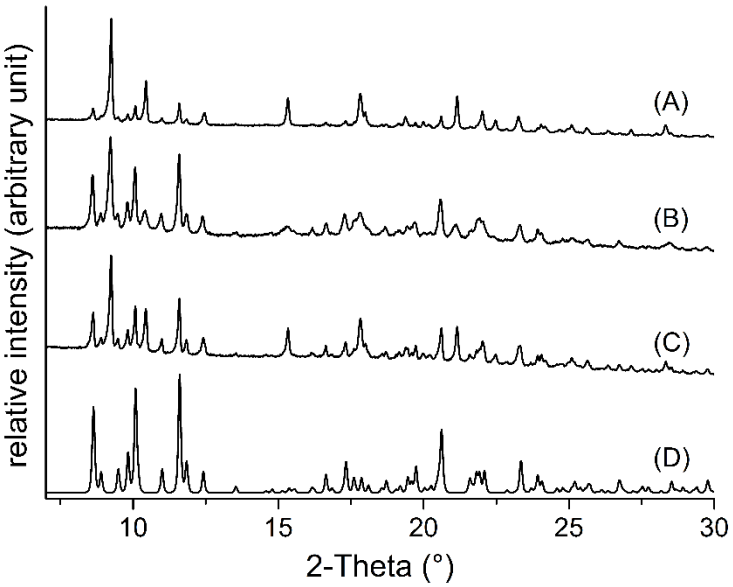

Figure S14. Experimental XRPD patterns of the residues obtained after the first mass loss with a heating rate of 1°C/min of **1-I** (A), **1-II** (B), **2** (C) and calculated XRPD pattern of **3-lc** (D).

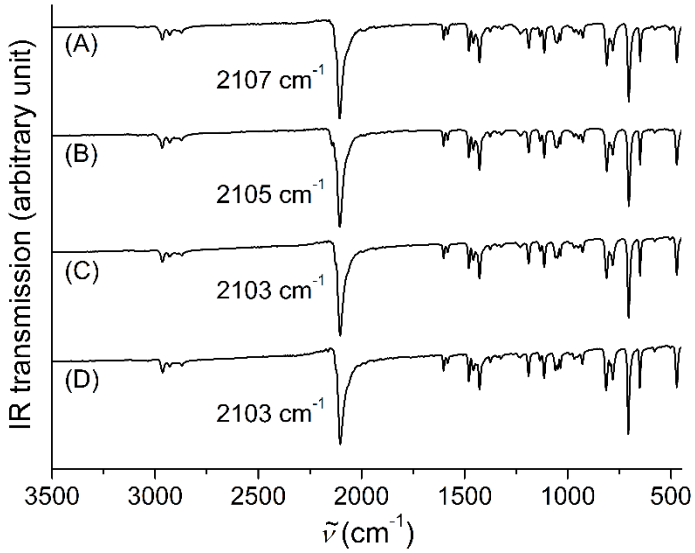

Figure S15. IR spectra of the residues obtained after the first mass loss in a TG measurement of **1-I** (A), **1-II** (B), **2** (C) and of **3-lc** (D). Given are the values for the CN stretching vibrations.

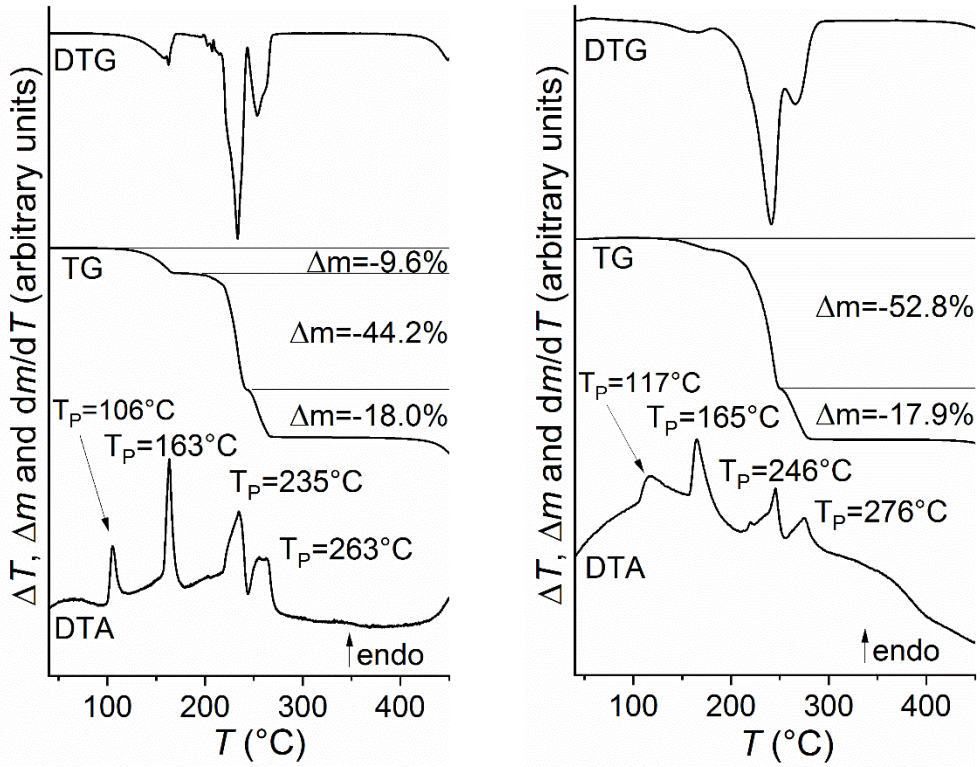

Figure S16. DTG, TG and DTA curve for **1-I** measured with a heating rate of 4 °C/min (left) and 16 °C/min (right).

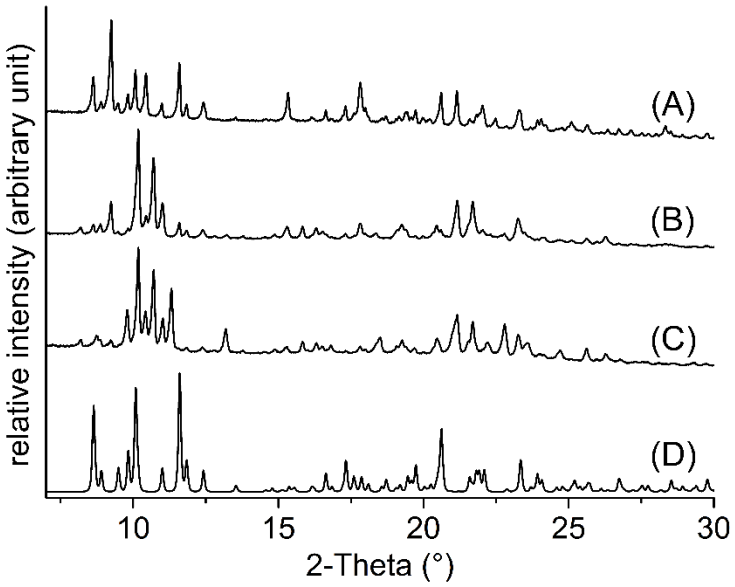

Figure S17. Experimental XRPD pattern of the residue obtained after the first mass loss in a TG measurement of **1-I** with a heating rate of 1°C/min (A), 4°C/min (B) and 16°C/min (C) as well as the calculated powder patterns **3-Ic** (D).

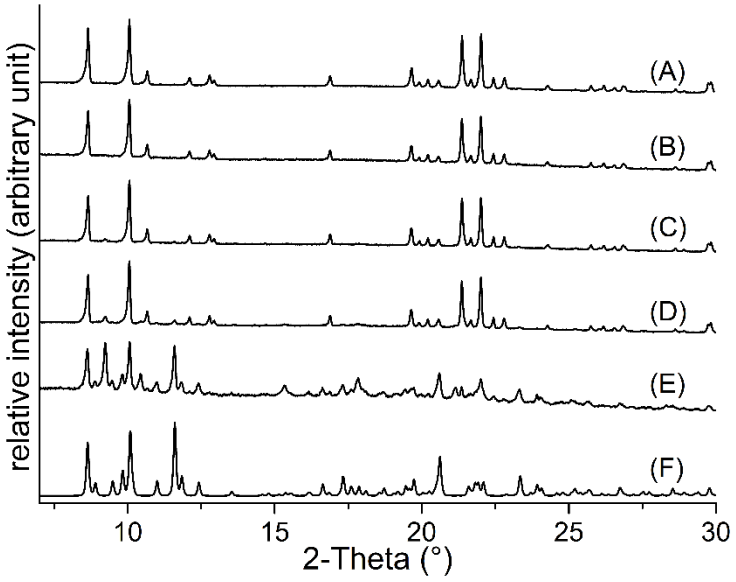

Figure S18. XRPD patterns of samples isolated at different reaction times by annealing **1-I** at 70°C for 2 (B), 6 (C), 24 (D) and 72 hours (E) as well as the calculated patterns of **1-I** (A) and **3-lc** (F).

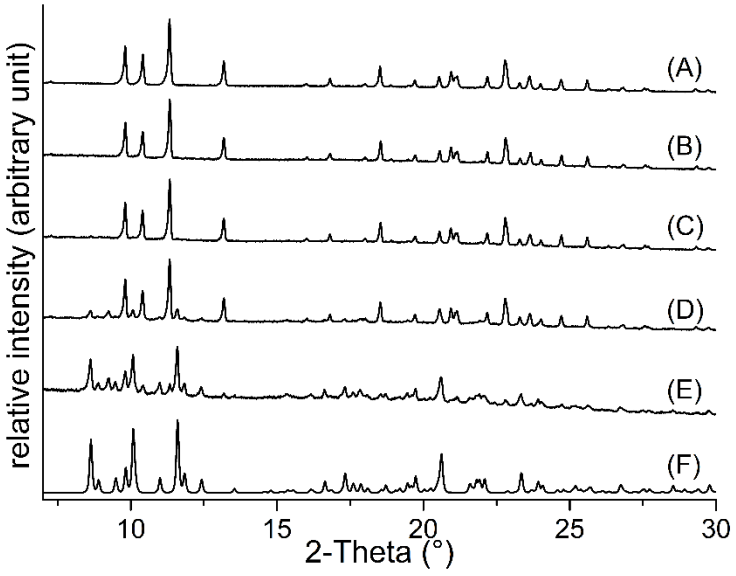

Figure S19. XRPD patterns of samples isolated at different reaction times by annealing **1-II** at 70°C for 2 (B), 6 (C), 24 (D) and 72 hours (E) as well as the calculated patterns of **1-II** (A) and **3-lc** (F).

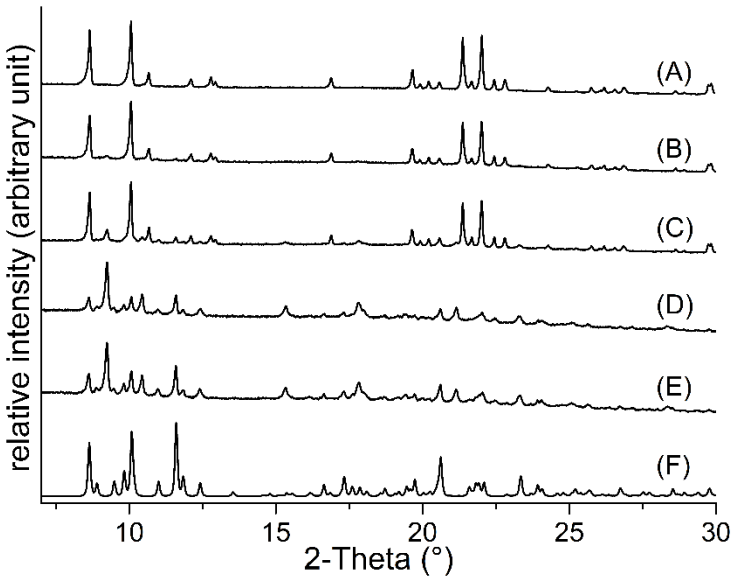

Figure S20. XRPD patterns of samples isolated at different reaction times by annealing **1-I** at 85°C for 2 (B), 6 (C), 24 (D) and 72 hours (E) as well as the calculated patterns of **1-I** (A) and **3-lc** (F).

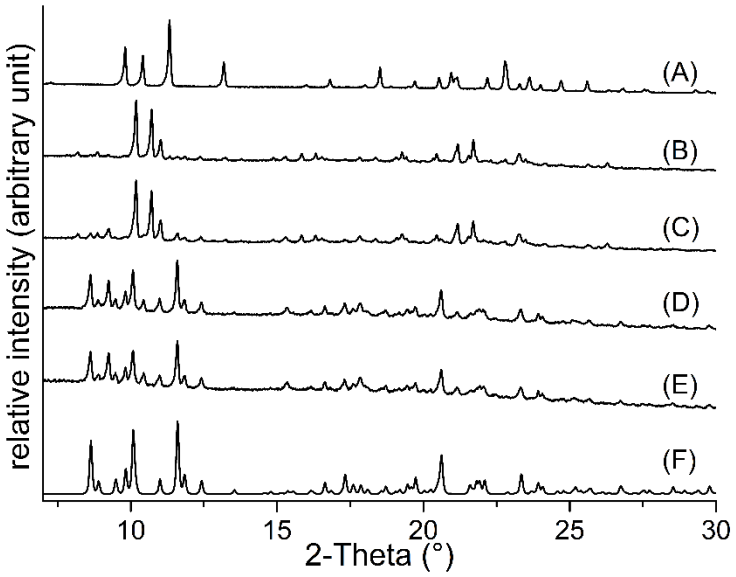

Figure S21. XRPD patterns of samples isolated at different reaction times by annealing **1-II** at 70°C for 2 (B), 6 (C), 24 (D) and 72 hours (E) as well as the calculated patterns of **1-II** (A) and **3-lc** (F).

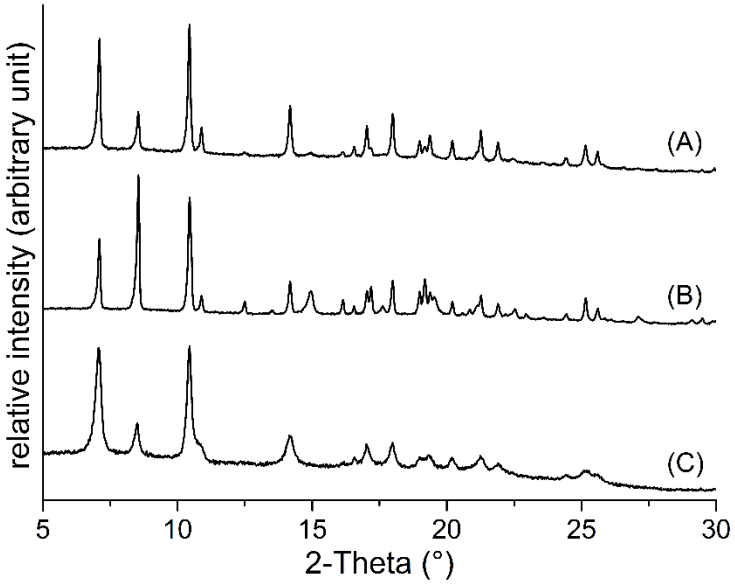

Figure S22. Experimental XRPD pattern of the residues obtained after the second mass loss with a heating rate of 1°C/min of **1-I** (A), **1-II** (B), **2** (C).

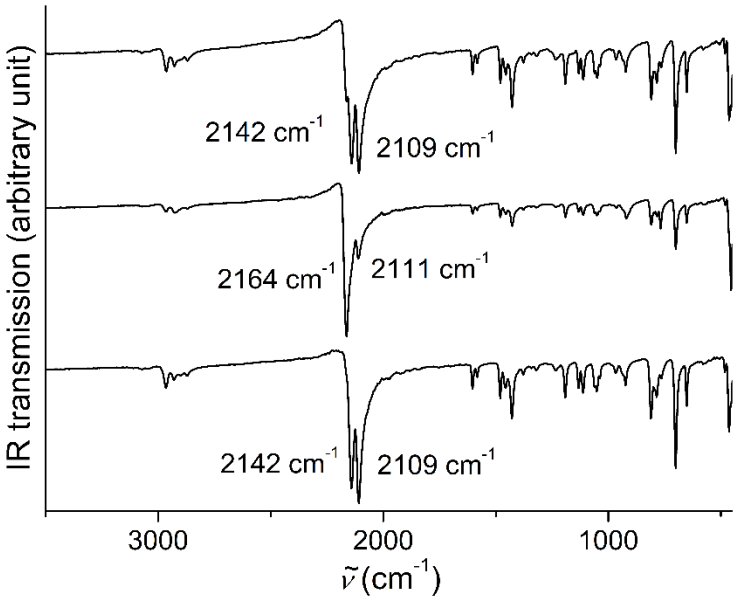

Figure S23. IR spectra of the residues obtained after the second mass loss in a TG measurement of **1-I** (A), **1-II** (B), **2** (C). Given are the values for the CN stretching vibrations.

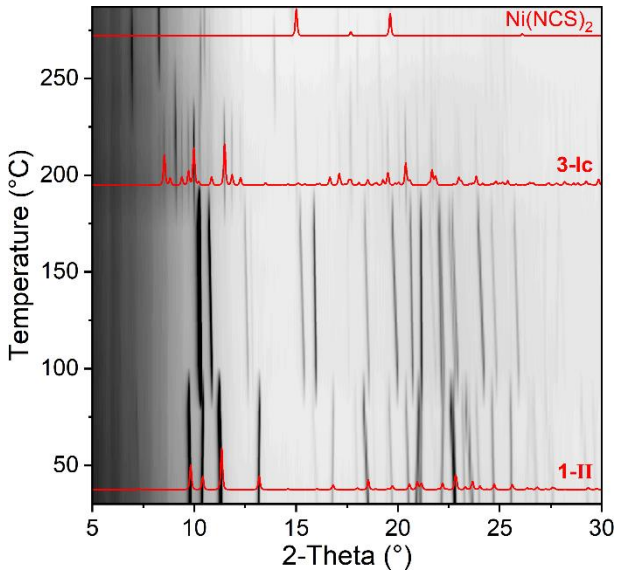

Figure S24. HTK measurement of **1-II** in an open capillary. The calculated powder pattern of **1-I**, **3-Ic** and $Ni(NCS)_2$ are given in red.

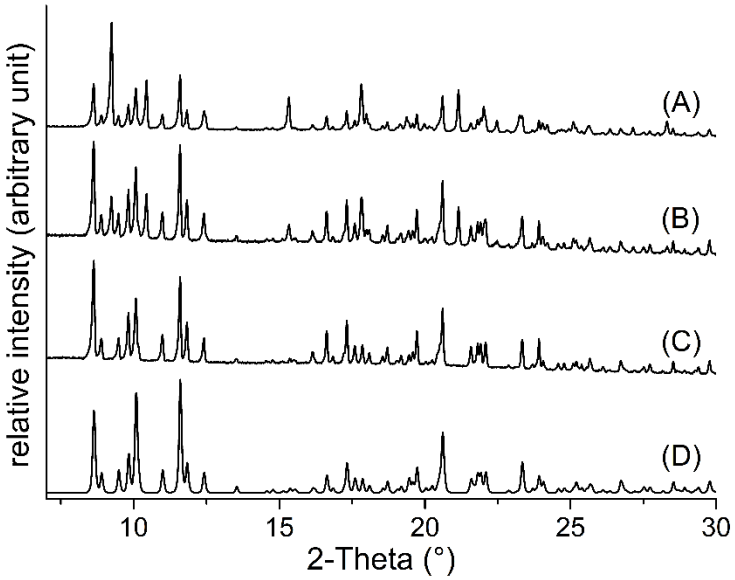

Figure S25. Experimental powder patterns of the residues that have formed if a mixture of **3-I** and **3-Ic** with excess of solid (A) is stirred in ethanol for 5 min (B) and 15 min (C) together with the calculated powder patterns of **3-Ic** (D).

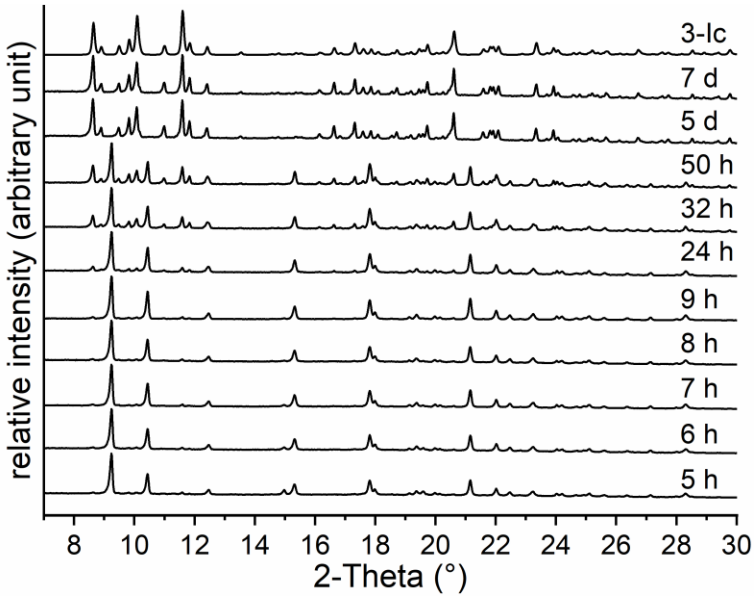

Figure S26. XRPD pattern of samples isolated at different reaction times if $Ni(NCS)_2$ is reacted with two equivalents of 3-ethylpyridine in ethyl acetate.

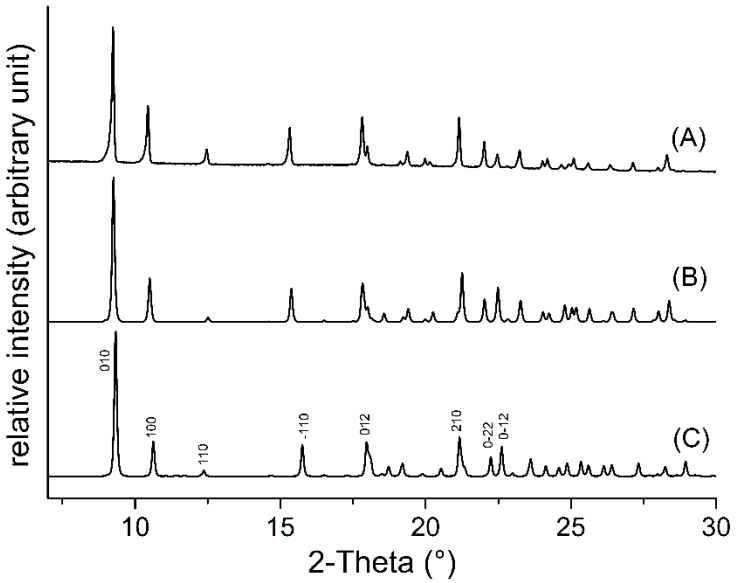

Figure S27. Experimental (A) and calculated XRPD pattern of **3-I** using the lattice parameters obtained from a pawley fit of a powder pattern measured at room temperature (B) and using the lattice parameters from single crystal data measured at 200 K (C).

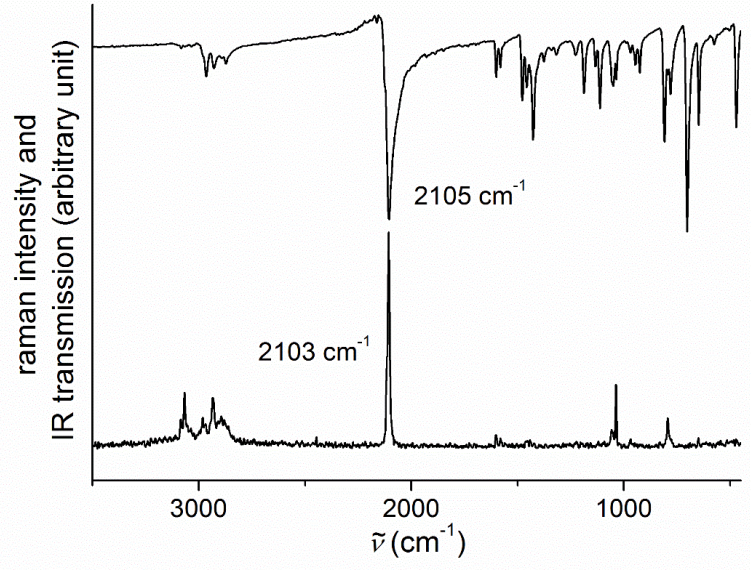

Figure S28. IR and Raman spectra of **3-I**. Given are the values for the CN stretching vibrations.

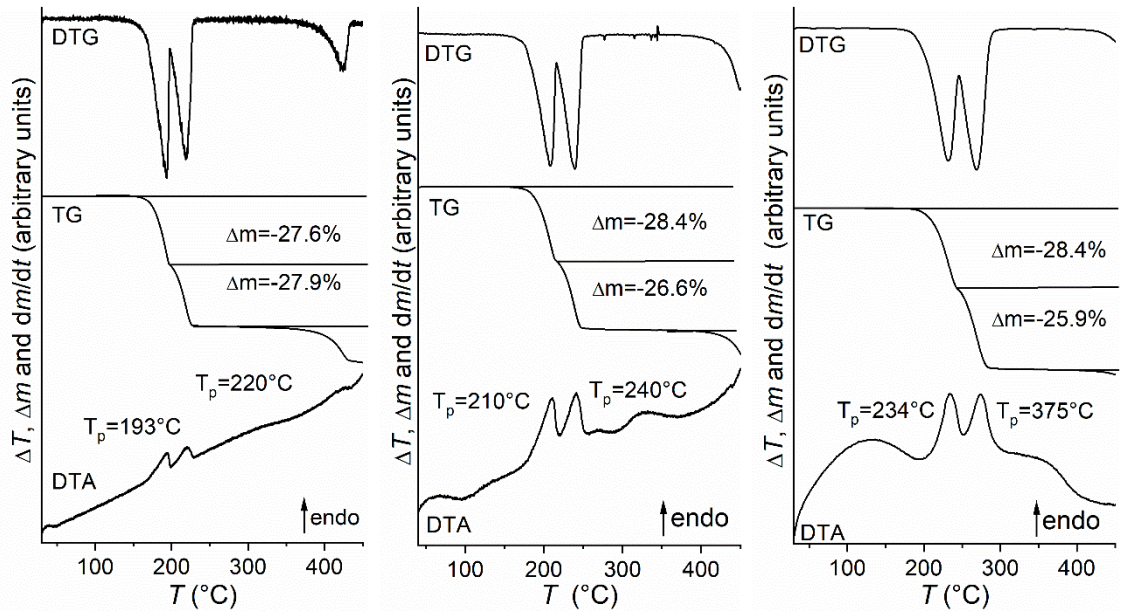

Figure S29. DTG, TG and DTA curve for **3-lc** measured with a heating rate of 1 (left), 4 (center) and 16 (right) °C/min.

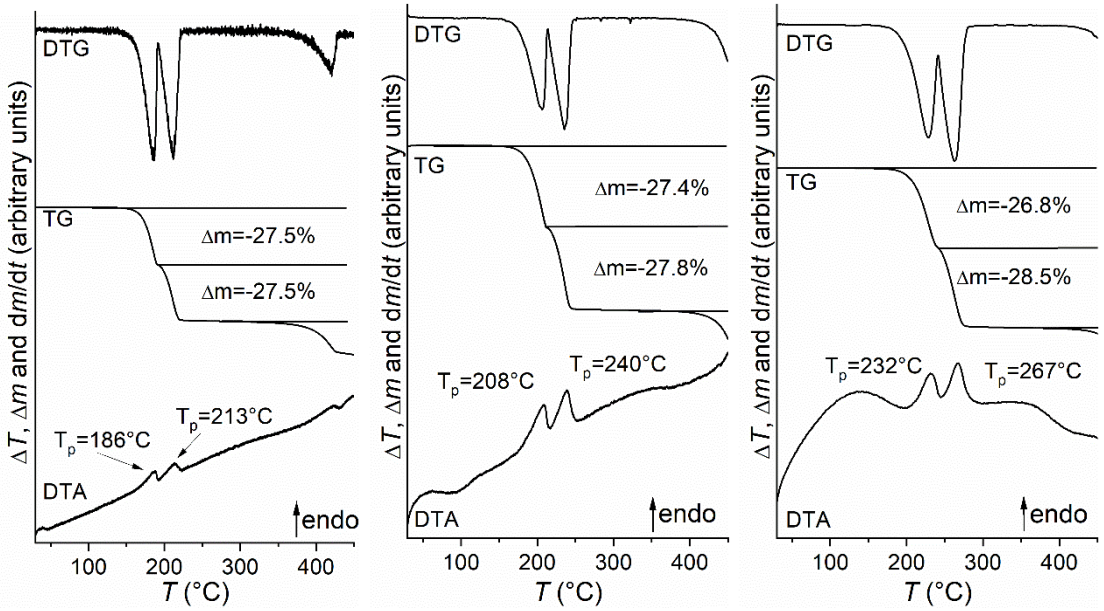

Figure S30. DTG, TG and DTA curve for **3-l** measured with a heating rate of 1 (left), 4 (center) and 16 (right) °C/min.

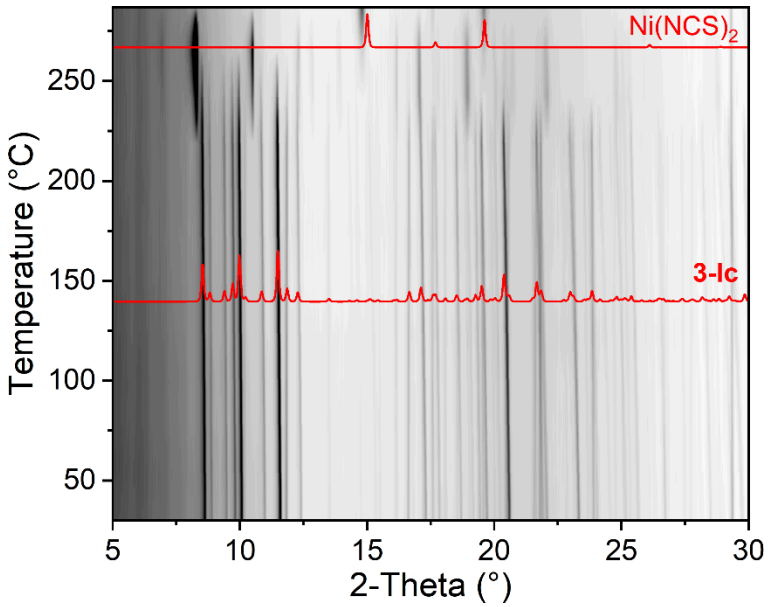

Figure S31. HTK measurement of **3-Ic** in an open capillary. The calculated powder pattern of **3-Ic** and $Ni(NCS)_2$ are given in red.

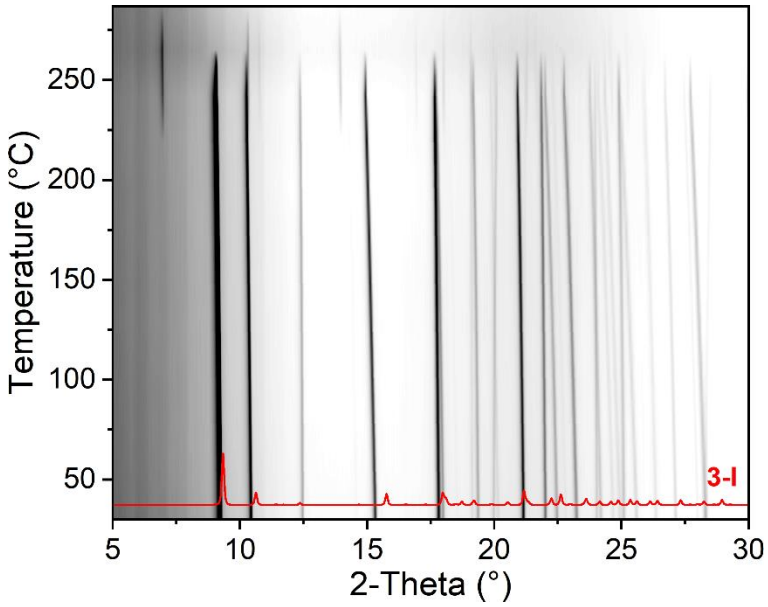

Figure S32. HTK measurement of **3-I** in an open capillary. The calculated powder pattern of **3-I** is given in red.

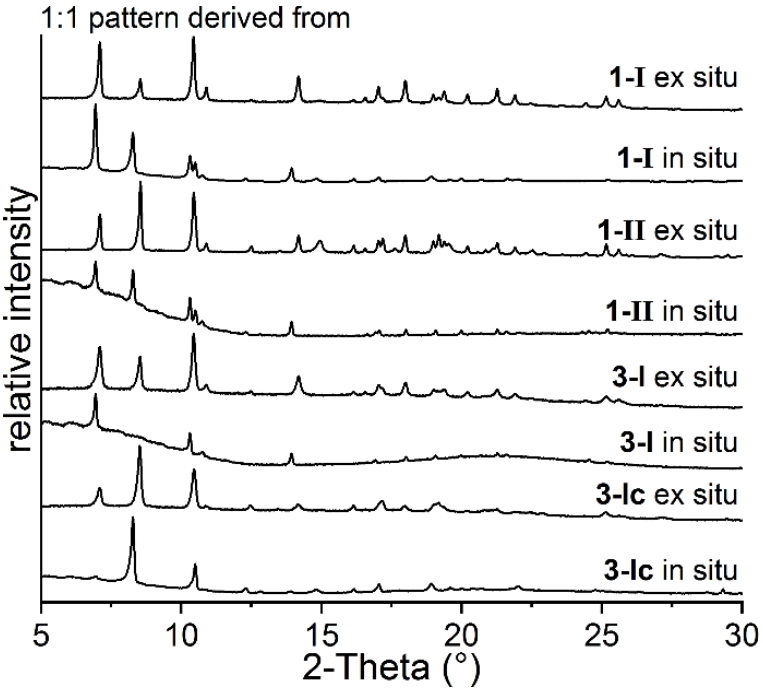

Figure S33. XRPD pattern of samples of $Ni(NCS)_2$(3-ethylpyridine) (**4**) synthesized by thermogravimetric measurements at 4°C/min (*ex situ*) or by temperature dependent XRPD measurements starting from **1-I**, **1-II**, **3-I** and **3-Ic** (in situ).

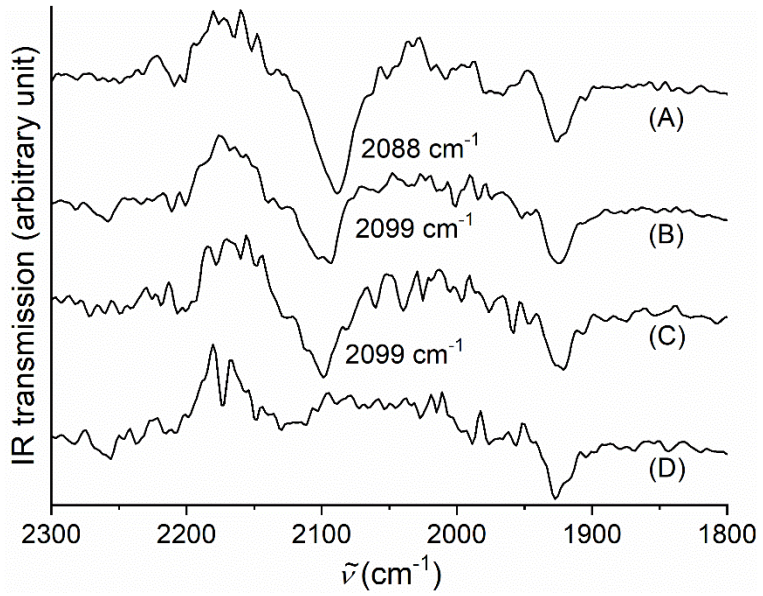

Fig S34. IR spectra of a solution of **1-I** (A), **3-I** (B), **3-Ic** (C) in ethanol (D). Given are the values for the CN stretching vibrations.

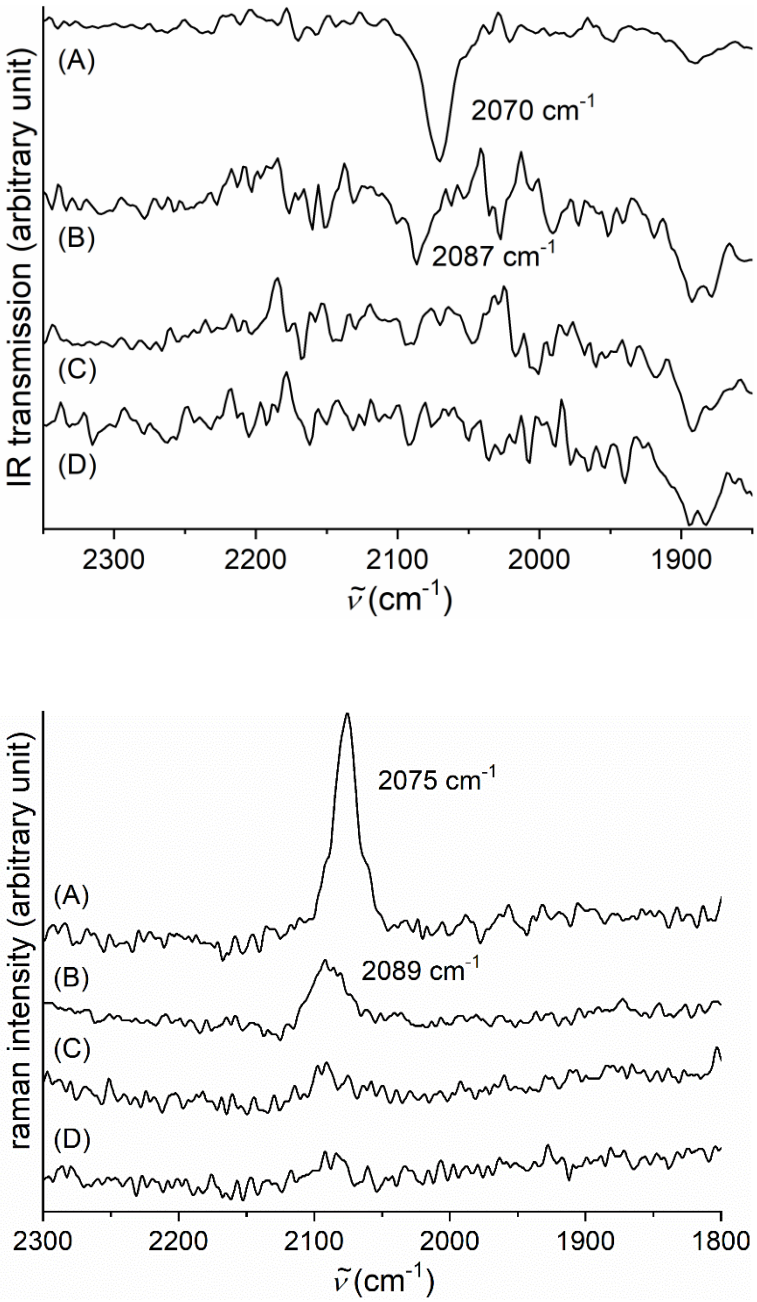

Fig S35. IR (top) and Raman spectra (bottom) of a solution of **1-I** (A), **3-l** (B), **3-lc** (C) in ethyl acetate (D). Given are the values for the CN stretching vibration.

Table S1. Selected crystal data and details of the single crystal structure refinements for **2**, **3-l**, **3-lc** and **3-CH_2Cl_2**.

compound	**2**	**3-l**	**3-lc**	**3-CH_2Cl_2**
Formula	$[Ni(NCS)_2(C_7H_9N)_2(H_2O)_2]$	$[Ni(NCS)_2(C_7H_9N)_2]$	$[Ni(NCS)_2(C_7H_9N)_2]$	$[Ni(NCS)_2(C_7H_9N)_2]\cdot(CH_2Cl)$
MW / g mol^{-1}	425.2	389.17	389.17	474.1
crystal system	*monoclinic*	*triclinic*	*triclinic*	*monoclinic*
space group	$P2_1/c$	P-1	P-1	C2/c
a / Å	9.114	9.310	10.103	16.813
b / Å	14.036	10.516	11.216	14.961
c / Å	7.883	11.057	18.545	9.801
α / °	90	68.06	106.44	90
β / °	100.88	66.94	94.39	114.89
γ / °	90	69.49	111.05	90
V / Å^3	990.31	897.0	1843.2	2236.36
T / K	200	200	200	200
Z	2	2	4	4
D_{calc} / g cm^{-3}	1.426	1.44	1.40	1.40
μ / mm^{-1}	1.207	1.32	1.28	1.30
θ_{max} / deg	26	26	27.044	26
measured refl.	7715	11792	17026	10318
unique refl.	1945	3511	7957	2193
R_{int}	0.1104	0.0241	0.0223	0.0218
refl. [$F_0>4\sigma(F_0)$]	1719	3042	6573	1967
parameters	117	220	418	116
R_1 [$F_0 > 4\sigma(F_0)$]	0.0583	0.0269	0.0341	0.0251
wR_2 [all data]	0.1566	0.0743	0.0928	0.0658
GOF	1.055	1.076	1.077	1.077
$\Delta\rho_{max/min}$ / e Å^{-3}	0.984 / -0.828	0.361 / -0.301	0.88 /-0.45	0.28 / -0.20

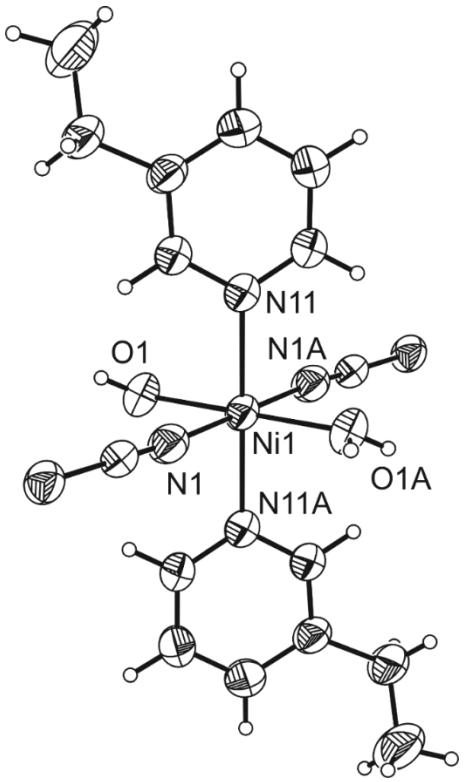

Figure S36. Crystal structure of **2** with labeling and displacement ellipsoids drawn at the 50% probability level.

Table S2. Selected bond lengths and angles for **2**. Symmetry transformations used to generate equivalent atoms: A: -x+1,-y+1,-z+1.

Ni1-N1A	2.047(3)	Ni1-N11A	2.101(2)
Ni1-N1	2.047(3)	Ni1-O1	2.112(2)
Ni1-N11	2.101(2)	Ni1-O1^{i}	2.112(2)
N1A-Ni1-N1	180.0	N11-Ni1-N11A	180.0
N1A-Ni1-N11	90.36(10)	N1A-Ni1-O1	91.83(9)
N1-Ni1-N11	89.64(10)	N1-Ni1-O1	88.17(9)
N1A-Ni1-N11A	89.64(10)	N11-Ni1-O1	91.73(9)
N1-Ni1-N11A	90.36(10)	N11A-Ni1-O1	88.27(9)
N1A -Ni1-O1A	88.17(9)	O1-Ni1-O1A	180.0
N1-Ni1-O1A	91.83(9)	C1-N1-Ni1	174.3(2)
N11-Ni1-O1A	88.27(9)	C15-N11-Ni1	121.82(19)
N11A -Ni1-O1A	91.73(9)	C11-N11-Ni1	121.02(18)

Table S3. Hydrogen bonds in **2**. Symmetry transformations used to generate equivalent atoms:
A: -x+1,-y+1,-z+1 B: x,-y+1/2, z-1/2 C: x,y,z-1.

D-H...A	d(D-H)	d(H...A)	d(D...A)	<(DHA)
C(11)-H(11)...S(1)B	0.95	3.01	3.902(3	156.8
O(1)-H(1A)...S(1)C	0.84	2.58	3.306(2)	144.8
O(1)-H(2A)...S(1)B	0.84	2.49	3.322(2	169.0

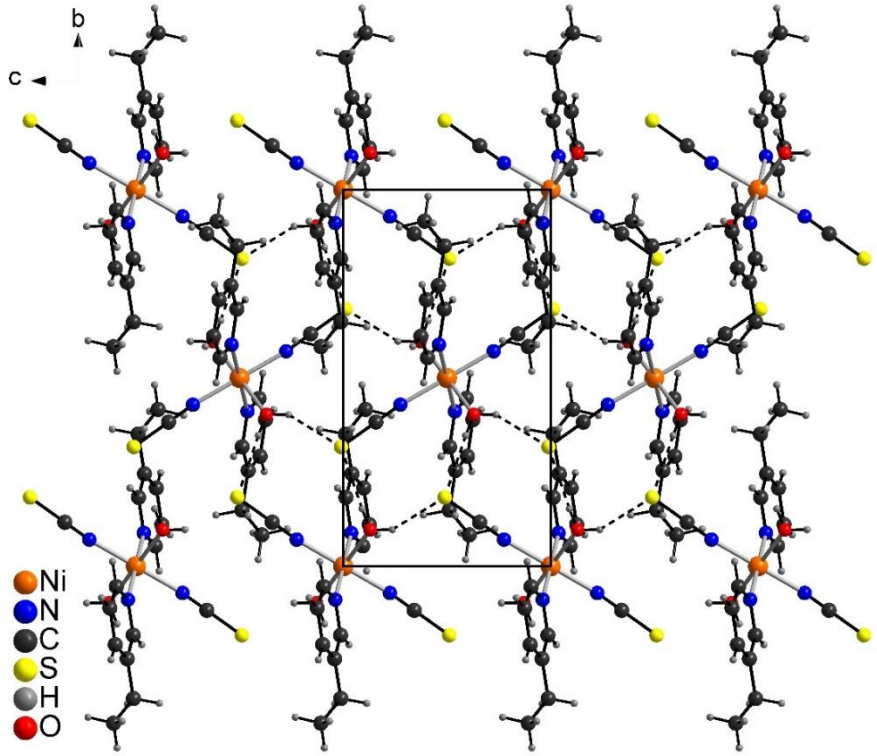

Figure S37. Crystal structure of **2** with view onto the layers along the crystallographic *a*-axis and intermolecular O-H···S hydrogen bonding shown as dashed lines.

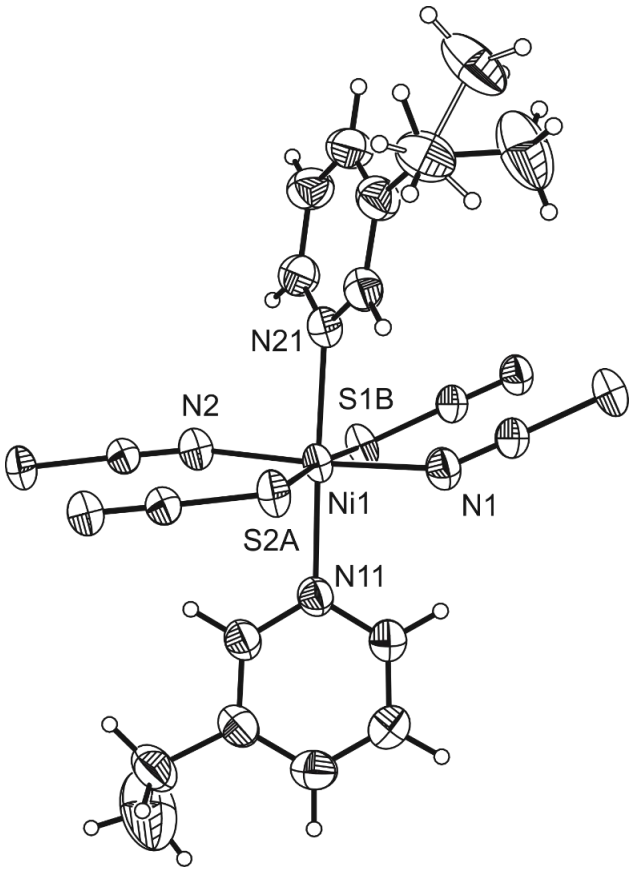

Figure S38. Crystal structure of **3-l** with labeling and displacement ellipsoids drawn at the 50% probability level. Symmetry transformations used to generate equivalent atoms: A -x+1,-y+1,-z+1 B -x+1,-y+1,-z+2.

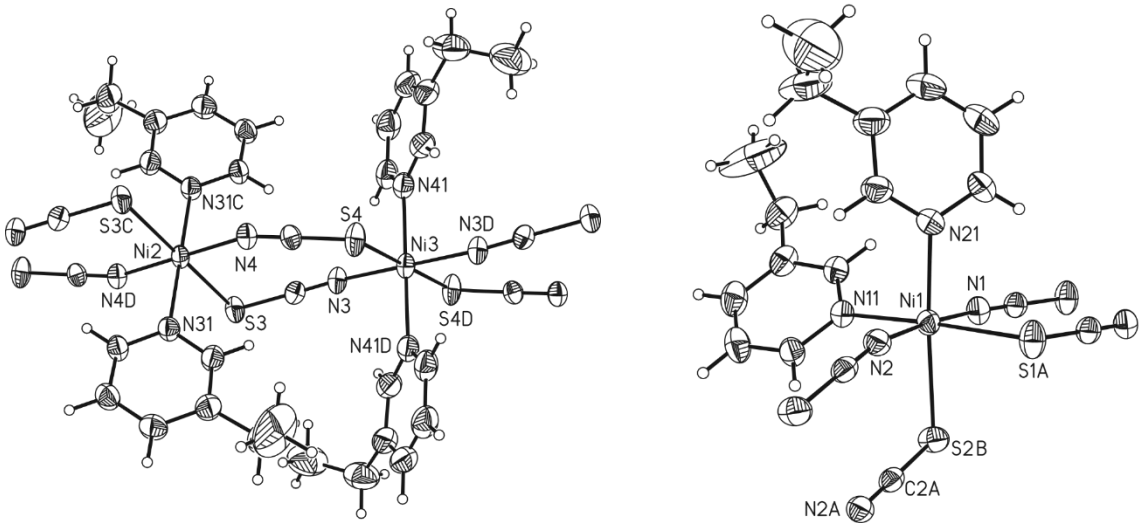

Figure S39. Crystal structure of **3-lc** with labeling and displacement ellipsoids drawn at the 50% probability level.

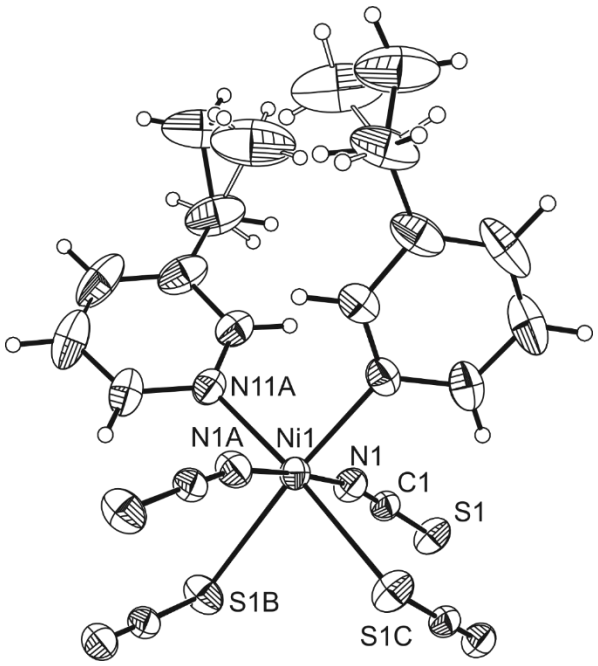

Figure S40. Crystal structure of **3-CH_2Cl_2** with labeling and displacement ellipsoids drawn at the 50% probability level.

Table S4. Selected bond lengths and angles for **3-CH_2Cl_2**. Symmetry transformations used to generate equivalent atoms: A: -x+1,y,-z+3/2; B: x,-y,z+1/2; C: -x+1,-y,-z+1.

Ni(1)-N(1)	2.0224(14)	Ni(1)-N(11)A	2.0848(14)
Ni(1)-N(1)A	2.0224(14)	Ni(1)-S(1)B	2.5726(5)
Ni(1)-N(11)	2.0847(14)	Ni(1)-S(1)C	2.5726(5)
N(1)-Ni(1)-N(1)A	176.28(8)	N(1)-Ni(1)-S(1)C	94.29(4)
N(1)-Ni(1)-N(11)	90.55(6)	N(1)A-Ni(1)-S(1)C	83.02(4)
N(1)A-Ni(1)-N(11)	92.01(6)	N(11)-Ni(1)-S(1)C	89.85(4)
N(1)-Ni(1)-N(11)A	92.01(5)	N(11)A-Ni(1)-S(1)C	173.02(4)
N(1)A-Ni(1)-N(11)A	90.55(6)	S(1)B-Ni(1)-S(1)C	87.94(2)
N(11)-Ni(1)-N(11)A	93.10(8)	C(1)-S(1)-Ni(1)C	99.92(5)
N(1)-Ni(1)-S(1)B	83.02(4)	C(1)-N(1)-Ni(1)	166.06(13)
N(1)A-Ni(1)-S(1)B	94.29(4)	C(11)-N(11)-Ni(1)	121.36(12)
N(11)-Ni(1)-S(1)B	173.02(4)	C(15)-N(11)-Ni(1)	120.34(13)
N(11)A-Ni(1)-S(1)B	89.85(4)		

Table S5. Selected bond lengths and angles for **3-I**. Symmetry transformations used to generate equivalent atoms: A: -x+1,-y+1,-z+1; B: -x+1,-y+1,-z+2.

3-I			
Ni(1)-N(2)	2.0293(18)	Ni(1)-N(21)	2.1290(17)
Ni(1)-N(1)	2.0397(17)	Ni(1)-S(2)A	2.5298(12)
Ni(1)-N(11)	2.1196(17)	Ni(1)-S(1)B	2.5361(12)
N(2)-Ni(1)-N(1)	175.66(6)	N(11)-Ni(1)-S(1)B	87.99(5)
N(2)-Ni(1)-N(11)	92.51(7)	N(21)-Ni(1)-S(1)B	91.56(5)
N(1)-Ni(1)-N(11)	91.57(7)	S(2)A-Ni(1)-S(1)B	175.852(19)
N(2)-Ni(1)-N(21)	89.36(7)	C(1)-N(1)-Ni(1)	152.25(14)
N(1)-Ni(1)-N(21)	86.57(7)	C(1)-S(1)-Ni(1)B	98.56(7)
N(11)-Ni(1)-N(21)	178.06(6)	C(2)-N(2)-Ni(1)	162.55(14)
N(2)-Ni(1)-S(2)A	93.36(5)	C(2)-S(2)-Ni(1)A	102.15(7)
N(1)-Ni(1)-S(2)A	85.30(5)	C(15)-N(11)-Ni(1)	120.28(13)
N(11)-Ni(1)-S(2)A	88.34(5)	C(11)-N(11)-Ni(1)	122.29(13)
N(21)-Ni(1)-S(2)A	92.04(5)	C(21)-N(21)-Ni(1)	121.97(13)
N(2)-Ni(1)-S(1)B	88.73(5)	C(25)-N(21)-Ni(1)	120.41(13)
N(1)-Ni(1)-S(1)B	92.87(5)		

Table S6. Selected bond lengths and angles for **3-Ic**.

3-Ic	Symmetry transformations used to generate equivalent atoms: A: -x+2,-y,-z B: -x+1,-y,-z C: -x+1,-y+1,-z+1 D: -x+1,-y,-z+1		
Ni(1)-N(1)	2.0288(18)	Ni(1)-N(11)	2.0984(18)
Ni(1)-N(2)	2.0292(18)	Ni(1)-S(1)A	2.5544(6)
Ni(1)-N(21)	2.0894(19)	Ni(1)-S(2)B	2.5574(7)
N(1)-Ni(1)-N(2)	175.64(8)	N(21)-Ni(1)-S(1)A	90.78(6)
N(1)-Ni(1)-N(21)	90.29(8)	N(11)-Ni(1)-S(1)A	173.12(5)
N(2)-Ni(1)-N(21)	93.28(7)	N(1)-Ni(1)-S(2)B	82.36(6)
N(1)-Ni(1)-N(11)	92.71(7)	N(2)-Ni(1)-S(2)B	94.07(5)
N(2)-Ni(1)-N(11)	89.75(7)	N(21)-Ni(1)-S(2)B	172.65(5)
N(21)-Ni(1)-N(11)	90.84(7)	N(11)-Ni(1)-S(2)B	89.32(5)
N(1)-Ni(1)-S(1)A	93.98(5)	S(1)A-Ni(1)-S(2)B	89.92(2)
N(2)-Ni(1)-S(1)A	83.48(5)	Ni(2)-N(31)	2.1210(18)
Ni(2)-N(4)C	2.0356(19)	Ni(2)-S(3)C	2.5246(6)
Ni(2)-N(4)	2.0356(19)	Ni(2)-S(3)	2.5247(6)
Ni(2)-N(31)C	2.1210(18)	N(31)C-Ni(2)-S(3)C	88.73(5)
N(4)C-Ni(2)-N(4)	180.00(11)	N(31)-Ni(2)-S(3)C	91.27(5)
N(4)C-Ni(2)-N(31)C	89.51(7)	N(4)C-Ni(2)-S(3)	87.29(5)
N(4)-Ni(2)-N(31)C	90.49(7)	N(4)-Ni(2)-S(3)	92.71(5)
N(4)C-Ni(2)-N(31)	90.49(7)	N(31)C-Ni(2)-S(3)	91.27(5)
N(4)-Ni(2)-N(31)	89.51(7)	N(31)-Ni(2)-S(3)	88.73(5)
N(31)C-Ni(2)-N(31)	180.0	S(3)C-Ni(2)-S(3)	180.0
N(4)C-Ni(2)-S(3)C	92.71(5)	Ni(3)-N(41)	2.115(2)
N(4)-Ni(2)-S(3)C	87.29(5)	Ni(3)-S(4)	2.5340(6)
Ni(3)-N(3)D	2.0387(19)	Ni(3)-S(4)D	2.5340(6)
Ni(3)-N(3)	2.0388(19)	N(41)D-Ni(3)-S(4)	90.14(6)
Ni(3)-N(41)D	2.115(2)	N(41)-Ni(3)-S(4)	89.86(6)
N(3)D-Ni(3)-N(3)	180.0	N(3)D-Ni(3)-S(4)D	93.15(6)
N(3)D-Ni(3)-N(41)D	90.62(8)	N(3)-Ni(3)-S(4)D	86.85(6)
N(3)-Ni(3)-N(41)D	89.38(8)	N(41)D-Ni(3)-S(4)D	89.86(6)
N(3)D-Ni(3)-N(41)	89.38(8)	N(41)-Ni(3)-S(4)D	90.14(6)
N(3)-Ni(3)-N(41)	90.62(8)	S(4)-Ni(3)-S(4)D	180.0
N(41)D-Ni(3)-N(41)	180.0	N(3)-Ni(3)-S(4)	93.15(6)
N(3)D-Ni(3)-S(4)	86.85(6)		

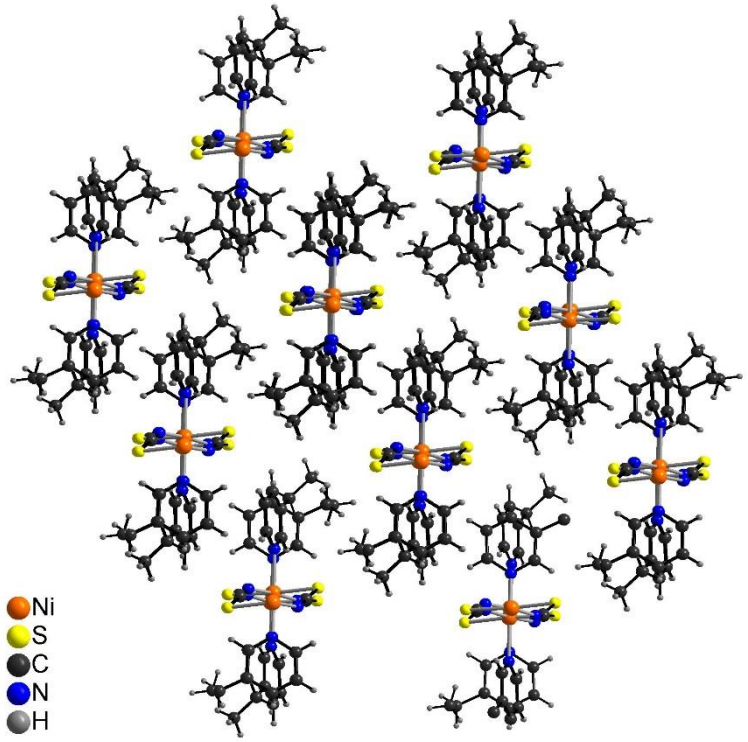

Figure S41. Crystal structure of **3-l** with view along the $Ni(NCS)_2$ chains.

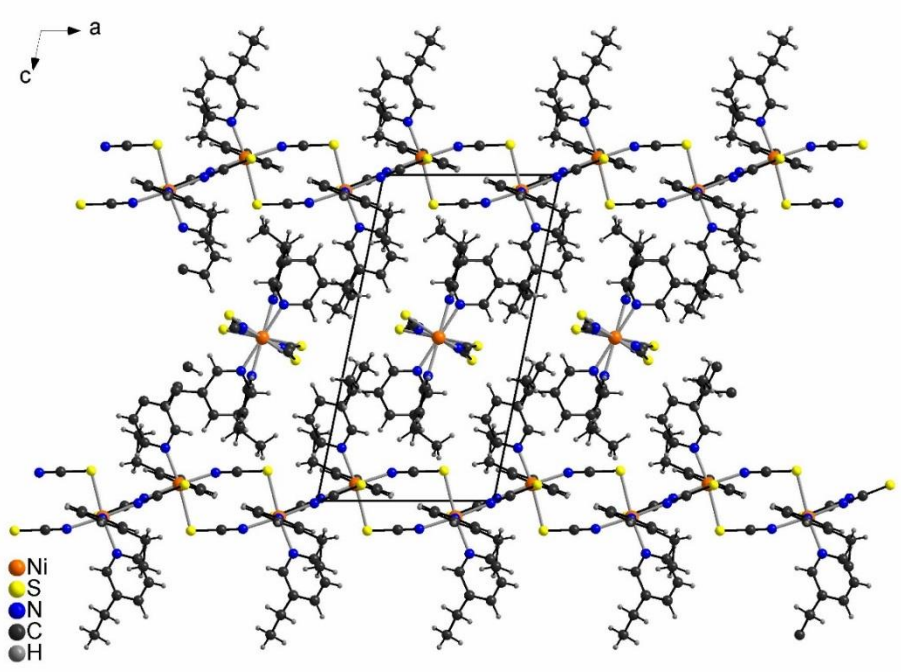

Figure S42. Crystal structure of **3-lc** with view along the crystallographic *b*-axis.

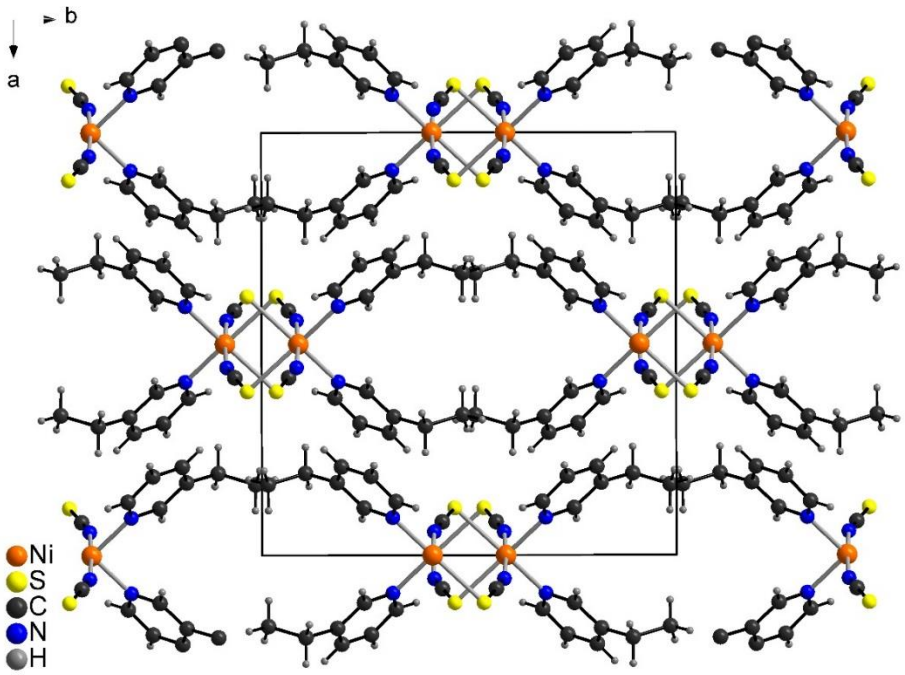

Figure S43. Crystal structure of **3-CH_2Cl_2** with view along the crystallographic *c*-axis.

Table S7. Hydrogen bonds in **3-I**, **3-Ic.**

D-H...A	d(D-H)	d(H...A)	d(D...A)	<(DHA)
3-I	Symmetry transformations used to generate equivalent atoms: A: -x+1,-y+1,-z+1 B: -x+1,-y+1,-z+2			
C(11)-H(11)...N(2)	0.95	2.53	3.097(3)	118.7
C(15)-H(15)...N(1)	0.95	2.45	3.016(3)	118.2
C(21)-H(21)...S(2)A	0.95	2.95	3.473(2)	116.0
C(25)-H(25)...S(1)B	0.95	2.94	3.392(3)	110.3
3-Ic	Symmetry transformations used to generate equivalent atoms: A: -x+2,-y,-z B: -x+1,-y,-z C: -x+1,-y+1,-z+1 D: -x+1,-y,-z+1			
C(35)-H(35)...N(4)C	0.95	2.67	3.128(3)	110.1
C(45)-H(45)...N(3)	0.95	2.68	3.136(4)	110.0